

Understanding Nanoparticle Porosity via Nanoimpacts and XPS: Electro-Oxidation of Platinum Nanoparticle Aggregates

Received 00th January 20xx,
Accepted 00th January 20xx

DOI: 10.1039/x0xx00000x

www.rsc.org/

Xue Jiao,^a Eden E. L. Tanner,^a Stanislav V. Sokolov,^a Robert G. Palgrave,^b Neil P. Young^c and Richard G. Compton^{a*}

The porosity of platinum nanoparticle aggregates (PtNPs) is investigated electrochemically via particle-electrode impacts and by XPS. The mean charge per oxidative transient is measured from nanoimpacts; XPS shows the formation of PtO and PtO₂ in relative amounts defined by the electrode potential and an average oxidation state is deduced as a function of potential. The number of platinum atoms oxidised per PtNP is calculated and compared with two models: solid and porous spheres, within which there are two cases: full and surface oxidation. This allows insight into extent to which the internal surface of the aggregate is 'seen' by the solution and is electrochemically active.

Introduction

Nanoparticles have diverse applications, both fundamental and applied, ranging from electrocatalysis, chemical and biochemical reactions to energy transformation and environmental remediation, due to their very high surface area compared to conventional materials.¹⁻⁸ The high surface area derives from the small geometric size of the particles leading to a high area to volume ratio which for solid spherical particles scales as the inverse of the particle radius. However, in addition, many nanoparticles are themselves composed of many smaller particles aggregated together. This feature gives the nanoparticles additional surface area reflecting the porosity of the individual aggregates and this in turn may lead to changes in environmental adsorption, optical properties and pseudocapacitor performance.⁹⁻¹⁶

Nanoporosities can be probed, traditionally, via *ex situ* gas adsorption isotherm measurements such as the Brunauer-Emmett-Teller (BET) method; molecules, such as nitrogen or argon, are used. Such measurements are invaluable for the application of porous nanoparticles for gas–solid studies, for example in catalysis or sensing, and a careful analysis of the measured adsorption isotherm may give insight into the shape and size of the particle pores as well as information about the total surface area covered by the adsorbate probe. Nevertheless when using nanoparticle aggregates in solution, the extent to which the internal surface area of the nanoparticles is accessible to solution and, for example, electrochemically active is an open question and may not reflect insights gleaned from gas–solid BET studies.

In the present study we use the nanoimpacts method to study the electrochemical oxidation of platinum nanoparticles which are themselves aggregates of much smaller particles which have porosities which can be seen but not quantified via transmission electron microscopy (TEM). In the nanoimpacts method¹⁷⁻²⁰ individual particles, in this case platinum nano-aggregates, suspended in aqueous solution from time to time collide with a microelectrode under potentiostatic control resulting in their oxidation (or reduction).²¹⁻²² In the work reported below for the case of platinum particles if a suitably positive potential is applied the formation of surface oxides results. The charge produced reflects the extent of the surface oxidation so revealing the extent to which internal surfaces are electroactive. In the case of platinum, the electro-oxidation is likely to produce both PtO and PtO₂ so complementary XPS measurements are performed to allow the interpretation of the impact data as a function of potential. Finally a comparison is made with similar nanoparticles 'tagged' with a redox active probe²³ but of a relatively large size compared to the species involved in platinum oxides.

Experimental

Chemicals

Perchloric acid (70%, HClO₄) and sodium perchlorate monohydrate (98%, NaClO₄ · H₂O) were obtained from Sigma-Aldrich, Dorset, U.K. Citrate-capped platinum nanoparticles (PtNPs) were provided by NanoComposix, San Diego, CA, U.S.A with a reported diameter 50 nm and concentration of 3.3 × 10¹³ particles L⁻¹.²⁴ All solutions were prepared with ultrapure water from Millipore with a resistivity of not less than 18.2 MΩ cm at 298 K.

Electrochemistry

A three electrode system in a Faraday cage was employed for all electrochemical experiments, with a μAutolab III (Metrohm Autolab B.V., Utrecht, The Netherlands) or an in-house potentiostat.²⁵ The working electrode was a glassy carbon (GC) macrodisk (3 mm diameter; BASi, West Lafayette, IN, U.S.A) or

^a Department of Chemistry, Physical and Theoretical Chemistry Laboratory, University of Oxford, South Parks Road, Oxford OX1 3QZ United Kingdom.

^b Department of Chemistry, University College London, 20 Gordon Street, London WC1H 0AJ, United Kingdom.

^c Department of Materials, University of Oxford, Parks Road, Oxford OX1 3PH, United Kingdom.

Electronic Supplementary Information (ESI) available: [details of any supplementary information available should be included here]. See DOI: 10.1039/x0xx00000x

a carbon fibre microdisc (33 μm diameter; BASi, West Lafayette, IN, U.S.A) electrode. Both electrodes were polished with alumina powders (Buehler, Lake Bluff, IL, U.S.A) in a size sequence: 1.0 μm , 0.3 μm and 0.05 μm . The reference electrode was a saturated calomel electrode (SCE) [$\text{Hg}/\text{Hg}_2\text{Cl}_2$, saturated KCl] (+ 0.241 V vs standard hydrogen electrode, SHE; BASi, West Lafayette, IN, U.S.A) or a silver/silver chloride electrode [Ag/AgCl , 1.0 M KCl] (+ 0.235 V vs SHE; Cypress Systems, Lawrence, KS, U.S.A) (this is used in the nanoimpact experiments to avoid leakage). The counter electrode was a graphite rod (6 mm diameter; Sigma-Aldrich, Dorset, U.K) or a platinum foil (Goodfellow, Cambridge, U.K). All experiments were conducted under a nitrogen atmosphere. All electrochemical measurements were thermostatted at 25 \pm 0.5 $^\circ\text{C}$.

In the experimental data reported below, potentials are quoted on the SCE or the Ag/AgCl (1.0 M KCl) scales.

Drop-Casting Experiments

The GC macroelectrode was modified by drop casting of a stock PtNP suspension (3 μL) onto the surface, which was subsequently allowed to dry under flowing nitrogen prior to experimentation.

Nanoimpact Experiments

An in-house built low noise potentiostat was employed for both potentiostatic control and impact current measurement.²⁵ Analogue to digital conversion was achieved by connecting a NI USB-6003 data acquisition (DAQ) device (National Instruments, Austin, TX, U.S.A) to a computer interface via USB. The DAQ device was controlled by a script written in Python 2.7, which was run through the IDE Canopy (Enthought, Austin, TX, U.S.A). A low-noise current amplifier LCA-4K-1G (FEMTO, Messtechnik GmbH, Germany) was used to measure the currents at the working electrode (running to ground), which is within a limited output bandwidth of two cascaded passive RC-filters (100 Hz). The outcoming signal was oversampled and converted from analogue to digital at a stream rate of 4 kHz by the DAQ device. A highly stabilized (1 kHz bandwidth) classic adder potentiostat²⁶ was selected to allow potentiostatic control. It is noted that for the reference buffer, a high quality operational amplifier, LMC6001 (Farnell, Leeds, U.K) with an ultra-low-input bias (25 fA) was adopted; and for the potential control at counter electrode a high

quality low-noise operational amplifier, AD797 (Farnell, Leeds, U.K) was employed.

Characterisation

Both stock PtNP and PtNP oxides were characterised via transmission electron microscopy (TEM) and X-ray photoelectron spectroscopy (XPS).

TEM

The size of PtNPs was determined by TEM (JEOL JEM-3000F FEGTEM; 300 kV accelerating voltage). A drop of the stock PtNP suspension (3.3×10^{13} particles L^{-1}) was deposited onto holey carbon grids (Agar Scientific, Stansted, U.K), and samples were dried in air prior to imaging. TEM images were then analysed using ImageJ software²⁷ (National Institutes of Health, U.S). As shown in Figure 1(a) and (b), each PtNP was an aggregate of much smaller nanoparticles (about 2.5 nm radius from TEM). In total, 165 PtNP aggregates were sized to give a mean radius of 24.3 ± 1.6 nm (Figure 1(c)). This agrees well with the reported value of 25 nm from the manufacturer. To clarify, this size was selected (50nm diameter) in order to guarantee a favourable signal-noise ratio.

XPS

XPS (Thermo K-alpha spectrometer; University College London) was carried out to measure the elemental composition of both PtNP and PtNP oxides. Samples were prepared by depositing a drop of the stock PtNP suspension (3.3×10^{13} particles L^{-1}) onto GC plates (SPI Supplies, West Chester, PA, U.S.A), followed by drying in air prior to cyclic voltammograms (CVs) and imaging. The CVs were conducted in an aqueous solution of 10.0 mM HClO_4 and 30.0 mM NaClO_4 , and scanned from 0 to various stopping potentials (from 1.5 to 2.0 V vs SCE) at a rate of 25 mV s^{-1} . The XPS instrument utilised a 72 W monochromated Al Kalpha X-ray source ($E = 1486.6$ eV) focused to a spot of 400 microns diameter at the sample surface. Charging was compensated for by use of a dual beam (electron and Ar^+ ion) flood gun. The electron energy analyser consists of a double focusing 180 degree hemisphere with mean radius of 125 mm, operated in constant analyser energy (CAE) mode, and a 128 channel position sensitive detector. The pass energy was set to 200 eV for survey scans and 50 eV for high resolution regions. The binding energy scale of the instrument is regularly calibrated using three points (Ag, Au,

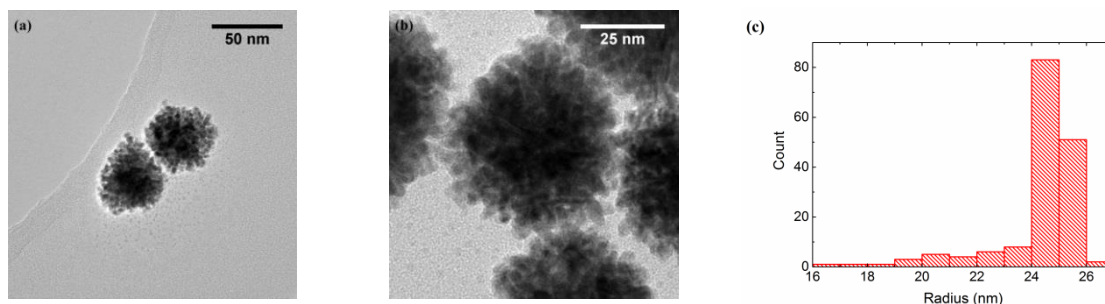


Figure 1(a) TEM bright field image of PtNPs. (b) High-resolution TEM image of one PtNP. (c) Size distribution of the PtNPs with an average radius of 24.3 ± 1.6 nm.

Cu). Spectra were analysed using the Thermo Avantage software.

To clarify, in this paper, "PtNP" refers to the platinum nanoparticle aggregate (ca. 25 nm radius), and "small nanoparticle" is the component of a PtNP (ca. 2.5 nm radius).

Results and Discussion

The porosity of PtNPs was established by analysing platinum oxidation using both electrochemical (cyclic voltammetry and nanoimpacts) and XPS techniques. First, cyclic voltammograms (CVs) were conducted; a glassy carbon (GC) macroelectrode was modified by drop casting a PtNP suspension and recording CVs. PtNPs were oxidised at different potentials, and XPS was used to detect different platinum oxides. Second, nanoimpact methodology was employed whereby overpotentials were applied to oxidise the PtNP aggregates and oxidative transients are observed. From these, the number of platinum atoms oxidised was calculated and compared with two theoretical models: a solid sphere, and a completely porous nanoparticle formed by aggregation of a large number of smaller particles. This therefore allows an estimation of the PtNP porosities.

Voltammetry, XPS and nanoimpact measurements

Experiments were conducted to explore the redox properties of PtNPs. First, a GC electrode was modified with stock PtNPs (Drop-Casting Experiments section) before being transferred to an aqueous solution of 10.0 mM HClO₄ and 30.0 mM NaClO₄. CVs were recorded and a reductive peak was obtained at ca. 1.8 V vs SCE, as shown in Figure 2. In the absence of PtNPs, no signal was observed (blue dashed line in Figure 2), indicating the peak was due to the PtNP oxidation. To clarify, this solution combination is selected to allow comparison with our previous work.²³

Next, XPS was performed to measure the elemental composition of platinum oxides. 7 samples were prepared by drop casting PtNPs on GC plate substrates; CVs were swept and stopped at different potentials from 1.50 to 2.00 V. XPS spectra were recorded in the 64-87 eV region corresponding to elemental platinum. The Pt 4f spectrum was fitted with up to three doublets. The Pt(0) peak was modelled with an asymmetric peak shape to account for the plasmon energy tailing in the metal, as has been observed previously for Pt(0) nanoparticles,²⁸ while higher oxidation states were modelled with symmetrical Gaussian-Lorentzian convolutions. Pt 4f_{7/2} components were found at binding energies of around 71.1 eV, corresponding to Pt(0), and 74.0 eV, corresponding to Pt(IV).²⁸⁻³⁰ An additional doublet was required with Pt 4f_{7/2} at around 71.8 eV binding energy, lower than expected for PtO₃ but similar to that reported for partially oxidised PtNPs.²⁸⁻²⁹ These environments cannot be unambiguously assigned to specific chemical species, for example they may be oxides or hydroxides, but are labelled here as Pt(0), Pt(II) and Pt(IV) in order of increasing binding energy. Table 1 and Figure 3 show that as the stopping potential increases, the amount of Pt(0) decreases and both Pt(II) and Pt(IV) increase. This gave an over-

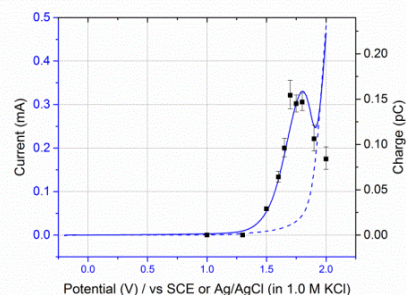
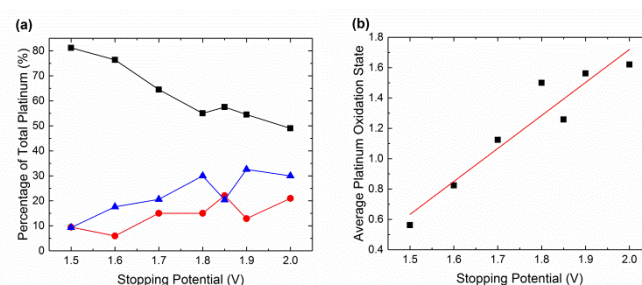


Figure 2 CVs for a GC macroelectrode with (blue solid line) or without (blue dashed line) PtNP modification. The variation of the average charge per impact transient, from overall 482 measurements, as a function of potential applied in the process of oxidation (black squares). All scans were performed in a nitrogen saturated solution of 10.0 mM HClO₄ and 30.0 mM NaClO₄, either at a scan rate of 25 mV s⁻¹ or



potentiostatted at various potentials.

Figure 3 (a) Elemental composition of platinum oxides at different stopping potentials: Pt(0) (black), Pt(II) (red) and Pt(IV) (blue). (b) Linear fit of average platinum oxidation state against stopping potentials with a reported coefficient of determination, R^2 , of 0.89.

CV Stopping Potential (V)	Criteria	Pt(0)	Pt(II)	Pt(IV)	Average Platinum Oxidation State
1.50	Amount	81.2	9.5	9.3	0.6
	BE (eV)	71.1	71.7	74.0	
1.60	Amount	76.4	6.0	17.6	0.8
	BE (eV)	71.2	71.9	74.1	
1.70	Amount	64.5	15.0	20.6	1.1
	BE (eV)	71.1	71.7	74.0	
1.80	Amount	55.0	15.0	30.0	1.5
	BE (eV)	71.1	71.7	74.0	
1.85	Amount	57.5	22.1	20.4	1.3
	BE (eV)	71.0	71.8	74.0	
1.90	Amount	54.5	12.9	32.6	1.6
	BE (eV)	71.0	71.6	74.2	
2.00	Amount	49.0	21.0	30.0	1.6
	BE (eV)	71.0	71.7	74.0	

Table 1 XPS analysis of PtNP oxidation.

rall increasing average platinum oxidation state, suggesting that, as expected, greater oxidation of the PtNPs occurs at higher overpotentials.

Next, nanoimpact measurements were conducted to investigate the oxidative charge per PtNP. Chronoamperograms (CAs) were recorded in an aqueous electrolyte of 10.0 mM HClO₄ and 30.0 mM NaClO₄ at various potentials (vs Ag/AgCl in 1.0 M KCl). In the experiments, 60 pM PtNPs were added and spikes were clearly observed of an approximate tens of millisecond duration, as shown in Figure 4 (black line). These are attributed to the platinum oxidation taking place when the nanoparticles make contact with the carbon fibre substrate. No impact spikes were observed in the case of electrolyte only, confirming that the oxidation of the PtNPs is the source of the transients.

The charge passed per transient (Q / C) was found to vary with the overpotential applied and reach a maximum at ca. 1.8 V as shown in Figure 2 (black squares). This is because the PtNPs were increasingly oxidised as the potential increased; at high potentials nonconductive oxide layers were formed on the surface of the nanoparticles, reducing any further reaction. This gave a peak at potential at ca. 1.8 V (vs Ag/AgCl in 1.0 M KCl). The XPS measurements showed the average platinum oxidation state increased consistently as the stopping potential increased to allow a further oxidation, so the reduced activity at high potentials may be related to the formation of PtO₂.

Calculation of the number of platinum atoms oxidised per PNP aggregate

A total of 482 spikes obtained at various potentials were analysed. A mean charge passed per impact transient (Q / C) was calculated at various overpotentials (Table 2),³¹ which is related to the number of platinum atoms oxidised (N_{Pt} / atom) via the electronic charge (e / C) according to

$$Q = neN_{Pt}$$

where n is the number of electron transferred during the process.

Hence the average number of platinum atoms per PtNP aggregate can be calculated at various potentials using the average platinum oxidation state from XPS. These can be further discussed and compared with the results from two simple geometric models (solid or porous spheres, see Figure 6), and within each model, two limiting extreme cases will be considered - full and surface oxidation. For full oxidation, all platinum atoms in the PtNP aggregates are oxidised; while for

Potential (V)	Average Charge per PtNP from Nanoimpact (pC) [±]	Average Platinum Oxidation State from XPS	Number of Platinum Atoms Oxidised per PtNP
1.50	0.03 [±] /1.07	0.6	3.1 × 10 ⁵
1.60	0.06 [±] /1.10	0.8	4.7 × 10 ⁵
1.65	0.10 [±] /1.11	-	-
1.70	0.15 [±] /1.11	1.1	8.5 × 10 ⁵
1.75	0.15 [±] /1.07	-	-
1.80	0.15 [±] /1.07	1.5	8.5 × 10 ⁵
1.85	-	1.3	-
1.90	0.11 [±] /1.14	1.6	4.3 × 10 ⁵
2.00	0.08 [±] /1.16	1.6	3.1 × 10 ⁵

Table 2 Average charge per PtNP aggregate from nanoimpact measurements.

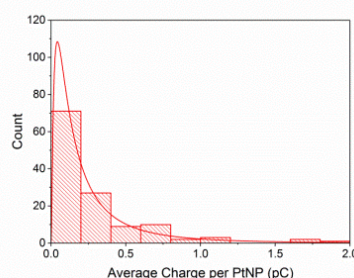


Figure 5 An example of transient charges at 1.70 V fitted with a lognormal distribution curve.



Model 1



Model 2

Figure 6 Two theoretical models of PtNPs.

surface oxidation, only those platinum atoms on the surface are oxidised.

Calculations were conducted for the following two geometric models where a close-packing arrangement was assumed for the platinum atoms or the small nanoparticles in the PtNP aggregates. In Model 1, each PtNP was a solid, smooth sphere

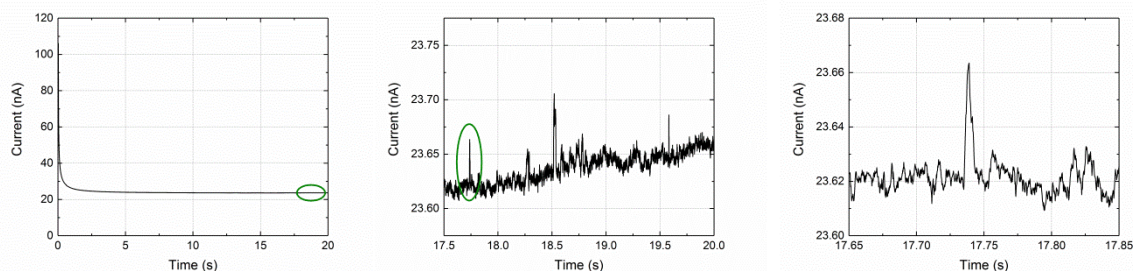


Figure 4 (a) CAs with 60 pM PtNPs; (b) A zoom of circled reductive transients in (a); (c) Further amplification of the circled spike in (b). All scans were recorded in a nitrogen saturated solution of 10.0 mM HClO₄ and 30.0 mM NaClO₄ and potentiostatted at various potentials (vs leakless Ag/AgCl in 1.0 M KCl).

of radius 25 nm; in Model 2, each PtNP (ca. 25 nm radius) was an aggregate of identical small nanoparticles (ca. 2.5 nm radius, estimated from Figure 2(b)). The number of platinum atoms oxidised can be obtained from both models for full and surface oxidation, and summarised in Table 3 (for details see ESI). To note, Model 1 was only calculated as a possible bound and in our experiments the particle was not fully oxidised.

At each potential, nanoimpacts was applied to determine the mean oxidative charge per PtNP; whilst XPS was used to deduce the number of electrons transferred via measurements of the mean platinum oxidation state. The number of platinum atoms oxidised was calculated and compared with the ones from solid (4.3×10^6 or 1.2×10^5 atoms for full and surface oxidation) and porous (3.2×10^6 or 8.8×10^5 atoms for full and surface oxidation) PtNP models (Table 3). There is a good estimation between the experimental result of peak current at 1.80 V (8.5×10^5) and the predicted value of the porous, surface model (8.8×10^5), suggesting a significant degree of porosity in the PtNPs used. The small difference may be because that in the process of oxidation, some of the platinum atoms on the surface of small nanoparticles were accessible whilst some were not. This is further confirmed by the TEM images, as clusters of small nanoparticles can be seen (Figure 1(a)), but the knowledge of their internal packing was limited. Finally we can compare the results from the oxidation of the porous platinum nano-aggregates with data obtained by the 'tagging' of the platinum surface with the redox active species nitrothiophenol (NTP) which irreversibly adsorbs at platinum. Nanoimpacts using the same NTP tagged platinum particles indicated that ca. 1.5×10^5 NTP molecules were adsorbed.²³ Approximating the adsorbate by a 'box' structure and using the following bond lengths (for N-O, C=C (aromatic) and C-H of 120, 140 and 100 pm) and van der Waals radii (for H, O, S of 120, 140 and 185 pm),³² the area occupied by one NTP molecule on the platinum surface lies between 2.4×10^{-19} and 3.3×10^{-19} m² per adsorbate. This suggests that each NTP molecule is associated with between 4.4 and 6 platinum atoms leading to an estimate of the number of surface platinum atoms 'seen' as being in the range 6.6×10^5 to 9.0×10^5 . This value is surprisingly consistent with the number determined from the platinum surface oxidation presented in the paper. Whilst the level of agreement is possibly to some extent fortuitous (approximations include a monolayer of platinum oxides only being formed) the methods both indicate a high level of particle porosity.

This result is significant as it investigates the porosity of nanoparticles using an easy, accessible direct redox process. The in situ methodology can be extended to other electrocatalytic reactions on any other nanomaterials, where the internal structure is essential to understand the full process.^{23, 33-37}

Number of Platinum Atoms Oxidised per PtNP	Full Oxidation	Surface Oxidation
Solid Sphere (Model 1)	4.3×10^6	1.2×10^5
Porous Sphere (Model 2)	3.2×10^6	8.8×10^5

Table 3 Number of platinum atoms oxidised per PtNP from two models (solid and porous), in the cases of full or surface oxidation.

Conclusions

In summary, PtNP aggregates with an internal structure of many ($10^2 - 10^3$) small nanoparticles can be investigated via direct electrochemical redox reactions. Nanoimpacts were applied, together with XPS, to explore the number of actively oxidised platinum atoms, which were essential in understanding the origin of their redox and catalytic properties.

Acknowledgements

The research is sponsored by the funding from the European Research Council under the European Union Seventh Framework Programme (FP/2007-2013) / ERC Grant Agreement n. [320403]. Xue Jiao thanks the China Scholarship Council for supporting her DPhil research.

Notes and references

‡ The transient charges from each potential were dispersed in a lognormal distribution (evidence shown in Figure 5), with the mean μ and the standard error of mean σ/\sqrt{n} , as measurements of the minimum current restricted by the potentiostat. To clarify, the "back-transformed" values in terms of charge (Q / C) can be written in a mathematical expression according to the lognormal law, with the median $\mu^* = e^\mu$ and the multiplicative standard error of mean $\sigma/\sqrt{n} = e^{\sigma/\sqrt{n}}$. Therefore the sign $\times/$ (times/divide) was employed to denote the error, analogous to the \pm notation used in a Gaussian distribution.

1. Taeho, K.; Taeghwan, H., Applications of inorganic nanoparticles as therapeutic agents. *Nanotechnology* **2014**, *25* (1), 012001.
2. Bandaru, P. R.; Yamada, H.; Narayanan, R.; Hofer, M., Charge transfer and storage in nanostructures. *Materials Science and Engineering: R: Reports* **2015**, *96*, 1-69.
3. Raimondi, F.; Scherer, G. G.; Kötzt, R.; Wokaun, A., Nanoparticles in Energy Technology: Examples from Electrochemistry and Catalysis. *Angewandte Chemie International Edition* **2005**, *44* (15), 2190-2209.

4. Tong, R.; Hemmati, H. D.; Langer, R.; Kohane, D. S., Photoswitchable Nanoparticles for Triggered Tissue Penetration and Drug Delivery. *Journal of the American Chemical Society* **2012**, *134* (21), 8848-8855.
5. Chen, A.; Holt-Hindle, P., Platinum-Based Nanostructured Materials: Synthesis, Properties, and Applications. *Chemical Reviews* **2010**, *110* (6), 3767-3804.
6. Chen, A.; La Russa, D. J.; Miller, B., Effect of the Iridium Oxide Thin Film on the Electrochemical Activity of Platinum Nanoparticles. *Langmuir* **2004**, *20* (22), 9695-9702.
7. Thearle, R. A.; Sofer, Z.; Bouša, D.; Pumera, M., Impact Electrochemistry: Detection of Graphene Nanosheets Labeled with Metal Nanoparticles through Oxygen Reduction Mediation. *ChemPhysChem* **2016**, *17* (13), 2096-2099.
8. Lim, C. S.; Tan, S. M.; Sofer, Z.; Pumera, M., Impact Electrochemistry of Layered Transition Metal Dichalcogenides. *ACS Nano* **2015**, *9* (8), 8474-8483.
9. Jung, H. B.; Xu, H.; Konishi, H.; Roden, E. E., Role of nano-goethite in controlling U(VI) sorption-desorption in subsurface soil. *Journal of Geochemical Exploration* **2016**, *169*, 80-88.
10. Chen, Y.; Ma, Q.; Jia, H.; Wang, Y., Hydrothermal synthesis of ZnS microspheres with highly effective photocatalytic and antibacterial properties. *Journal of Materials Science: Materials in Electronics* **2016**, *27* (10), 10237-10243.
11. Liu, J.; Wang, Z.; Sheng, A.; Liu, F.; Qin, F.; Wang, Z. L., In Situ Observation of Hematite Nanoparticle Aggregates Using Liquid Cell Transmission Electron Microscopy. *Environmental Science & Technology* **2016**, *50* (11), 5606-5613.
12. Sokolov, S. V.; Tschulik, K.; Batchelor-McAuley, C.; Jurkschat, K.; Compton, R. G., Reversible or Not? Distinguishing Agglomeration and Aggregation at the Nanoscale. *Analytical Chemistry* **2015**, *87* (19), 10033-10039.
13. Ni, B.; Wang, X., Nanostructure formation via post growth of particles. *CrystEngComm* **2015**, *17* (36), 6796-6808.
14. Chang, E. P.; Evans, J. S., Pif97, a von Willebrand and Peritrophin Biomaterialization Protein, Organizes Mineral Nanoparticles and Creates Intracrystalline Nanochambers. *Biochemistry* **2015**, *54* (34), 5348-5355.
15. Wang, D.; Schaaf, P. Germany Pat., DE 102014003993, 2015.
16. Lang, X.; Hirata, A.; Fujita, T.; Chen, M., Three-Dimensional Hierarchical Nanoporosity for Ultrahigh Power and Excellent Cyclability of Electrochemical Pseudocapacitors. *Advanced Energy Materials* **2014**, *4* (10), 1301809-n/a.
17. Cheng, W.; Compton, R. G., Electrochemical detection of nanoparticles by 'nano-impact' methods. *TrAC Trends in Analytical Chemistry* **2014**, *58*, 79-89.
18. Pumera, M., Impact Electrochemistry: Measuring Individual Nanoparticles. *ACS Nano* **2014**, *8* (8), 7555-7558.
19. Rees, N. V., Electrochemical insight from nanoparticle collisions with electrodes: A mini-review. *Electrochemistry Communications* **2014**, *43*, 83-86.
20. Robbs, P. H.; Rees, N. V., Nanoparticle electrochemistry. *Physical Chemistry Chemical Physics* **2016**, *18* (36), 24812-24819.
21. Zhou, Y.-G.; Haddou, B.; Rees, N. V.; Compton, R. G., The charge transfer kinetics of the oxidation of silver and nickel nanoparticles via particle-electrode impact electrochemistry. *Physical Chemistry Chemical Physics* **2012**, *14* (41), 14354-14357.
22. Giovanni, M.; Ambrosi, A.; Sofer, Z.; Pumera, M., Impact electrochemistry of individual molybdenum nanoparticles. *Electrochemistry Communications* **2015**, *56*, 16-19.
23. Jiao, X.; Sokolov, S. V.; Tanner, E. E. L.; Young, N. P.; Compton, R. G., Exploring nanoparticle porosity using nano-impacts: platinum nanoparticle aggregates. *Physical Chemistry Chemical Physics* **2017**, *19* (1), 64-68.
24. NanoComposix 50 nm Citrate NanoXact™ Platinum Nanoparticles (Certificate of Analysis Examples): <http://50.87.149.212/Specification%20Sheets/Platinum%20Spec%20Sheets/PT50-NX-CIT-MGM1553.pdf?2581746>.
25. Batchelor-McAuley, C.; Ellison, J.; Tschulik, K.; Hurst, P. L.; Boldt, R.; Compton, R. G., In situ nanoparticle sizing with zeptomole sensitivity. *Analyst* **2015**, *140* (15), 5048-5054.
26. Souto, R. M., Electronic configurations in potentiostats for the correction of ohmic losses. *Electroanalysis* **1994**, *6* (7), 531-542.
27. Broeke, J.; Perez, J. M. M.; Pascau, J., *Image Processing with ImageJ*. Packt Publishing: 2015.
28. Dablemont, C.; Lang, P.; Mangeney, C.; Piquemal, J.-Y.; Petkov, V.; Herbst, F.; Viau, G., FTIR and XPS Study of Pt Nanoparticle Functionalization and Interaction with Alumina. *Langmuir* **2008**, *24* (11), 5832-5841.
29. Şen, F.; Gökağaç, G., Different Sized Platinum Nanoparticles Supported on Carbon: An XPS Study on These Methanol Oxidation Catalysts. *The Journal of Physical Chemistry C* **2007**, *111* (15), 5715-5720.
30. Bancroft, G. M.; Adams, I.; Coatsworth, L. L.; Bennewitz, C. D.; Brown, J. D.; Westwood, W. D., ESCA study of sputtered platinum films. *Analytical Chemistry* **1975**, *47* (3), 586-588.
31. Limpert, E.; Stahel, W. A.; Abbt, M., Log-normal Distributions across the Sciences: Keys and Clues On the charms of statistics, and how mechanical models resembling gambling machines offer a link to a handy way to characterize log-normal distributions, which can provide deeper insight into variability and probability—normal or log-normal: That is the question. *BioScience* **2001**, *51* (5), 341-352.
32. Haynes, W. M., *CRC Handbook of Chemistry and Physics, 97th Edition*. CRC Press: 2016.
33. Guo, Z.; Percival, S. J.; Zhang, B., Chemically Resolved Transient Collision Events of Single Electrocatalytic Nanoparticles. *Journal of the American Chemical Society* **2014**, *136* (25), 8879-8882.
34. Ahn, H. S.; Bard, A. J., Single-Nanoparticle Collision Events: Tunneling Electron Transfer on a Titanium Dioxide Passivated n-Silicon Electrode. *Angewandte Chemie International Edition* **2015**, *54* (46), 13753-13757.
35. Kim, J.; Kim, B.-K.; Cho, S. K.; Bard, A. J., Tunneling Ultramicroelectrode: Nanoelectrodes and Nanoparticle Collisions. *Journal of the American Chemical Society* **2014**, *136* (23), 8173-8176.
36. Bigall, N. C.; Härtling, T.; Klose, M.; Simon, P.; Eng, L. M.; Eychmüller, A., Monodisperse Platinum Nanospheres with Adjustable Diameters from 10 to 100 nm: Synthesis and Distinct Optical Properties. *Nano Letters* **2008**, *8* (12), 4588-4592.
37. Guo, H.; Liu, X.; Bai, C.; Chen, Y.; Wang, L.; Zheng, M.; Dong, Q.; Peng, D.-L., Effect of Component Distribution and Nanoporosity in CuPt Nanotubes on Electrocatalysis of the Oxygen Reduction Reaction. *ChemSusChem* **2015**, *8* (3), 486-494.